JACS
JOURNAL OF THE AMERICAN CHEMICAL SOCIETY

Article

pubs.acs.org/JACS

Planarization, Fusion, and Strain of Carbon-Bridged Phenylenevinylene Oligomers Enhance π-Electron and Charge Conjugation: A Dissectional Vibrational Raman Study

Paula Mayorga Burrezo,[†] Xiaozhang Zhu,[‡] Shou-Fei Zhu,[‡] Qifan Yan,[‡] Juan T. López Navarrete,*[,†] Hayato Tsuji,*[,‡,§] Eiichi Nakamura,*[,‡] and Juan Casado*[,†]

[†]Department of Physical Chemistry, University of Málaga, Campus de Teatinos s/n, Málaga 29071, Spain

[‡]Department of Chemistry, School of Science, The University of Tokyo, Hongo, Bunkyo-ku, Tokyo 113-0033 Japan

[§]JST-PRESTO, 4-1-8 Honcho, Kawaguchi, Saitama 332-0012, Japan

Supporting Information

ABSTRACT: We have used Raman spectroscopy to study the molecular and electronic structures of the radical cations and dications of carbon-bridged oligo(*para*-phenylenevinylene)s (**COPV*n***, n = 1−6) possessing consecutive fused pentagons and hexagons, up to 19, along with COPV derivatives having electron-donating and -withdrawing groups. This study was made possible by the outstanding stability of the charged states of COPVs. We could untangle the effects of π-conjugation in the planar structure on the Raman frequency by distinguishing it from other structural effects, such as strain in the vinylene groups shared by the two pentagons. The analyses showed that the radical cations have benzo-quinoidal structures confined in the center of the molecule, as well as benzo-aromatic rings at the terminal sites. In contrast, dications of **COPV*n*** longer than n = 3 exhibit a biradicaloid character because of the recovery of aromaticity in the central rings and quinoidal rings at the terminal positions. These biradicaloids favor a singlet nature in their ground electronic states because of the double spin polarization. The introduction of electron-donating and -withdrawing groups on the termini of a COPV core affords, upon oxidation or reduction, a fully delocalized class III mixed valence system because of the high degree of conjugation of the COPV platform, which favors extensive charge delocalization.

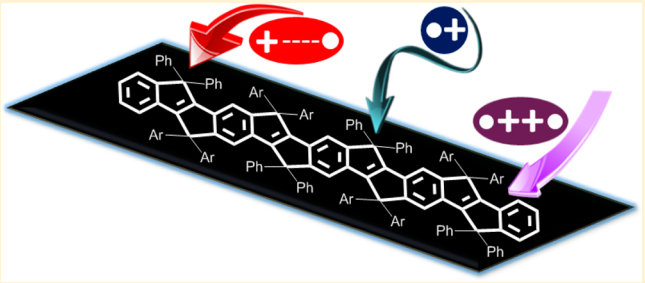

INTRODUCTION

Phenylenevinylene oligomers (OPVs) and polymers (PPVs) have been widely used in organic electronics since the discovery at an early stage of organic light-emitting diodes (OLEDs), bulk heterojunction solar cells,[1,2] and molecular wires,[3] where the torsional flexibility of the C−C bonds between phenylene and vinylene groups has been recognized as a cause of inefficient photonic performance and chemical instability.[1−4] The torsional motions also hamper in-depth studies on the electronic structure of these conjugated systems in their ground state and, in particular, of their charged species (i.e., *polaronic* radical cations, *bipolaronic* dications, *polaron-pair* dications, and higher oxidation states), which are necessary for gaining insights into such important effects as electron−electron correlation, spin−spin interactions, and electron−vibration couplings in this class of organic conducting materials.

We recently developed a general synthesis of the series of carbon-bridged oligo(*para*-phenylenevinylene)s illustrated in Scheme 1 (denoted as **COPV*n***). These molecules represent a family of OPV oligomers featuring fusion of consecutive six- and five-membered carbocycles, from four in **COPV1** up to 19 in **COPV6**,[5,6] and, consequently, a fully planar π-electron framework that allows a delocalized wave function free of conformational (electronic) disruptions.[7] They also feature a built-in ring strain caused by the presence of a vinylene group shared by two five-membered rings within a bicyclo[3.3.0]-octene skeleton. The strain activates the ground state and facilitates the formation of charged and excited states (see Scheme 1). The synergy of the planarity and the strain in the π-system have brought about some useful and unusual photophysical and electronic properties, such as intense light absorption, photoluminescence with a quantum yield of unity, and high photoinduced electron transfer rate from donor to acceptor when acting as molecular wires,[8] as well as high stability of the charged species, such as radical cations and dications. The 4-octylphenyl/phenyl groups standing orthogonal to the π-system keep the molecules away from each other in solution and in the solid state[5] and hence are also responsible for some of the above properties. Because the charged OPV/PPV systems are rarely available in stable forms, we considered that a Raman study of the charged states of the flat COPV molecules would provide fundamental information on the

Received: December 10, 2014
Published: March 2, 2015

DOI: 10.1021/ja5125463
J. Am. Chem. Soc. 2015, 137, 3834−3843

Scheme 1. Chemical Structures of the COPV Compounds[a]

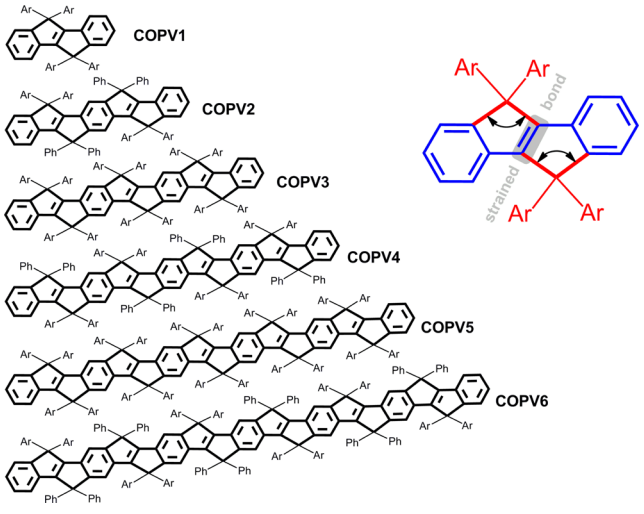

[a]**COPV1** to **COPV6** from the top to the bottom. Ar = 4-octylphenyl, Ph = phenyl.

electronic structure of π-conjugated systems in their polaronic and bipolaronic forms and related states.

In this article, we report on the electron and charge conjugation/delocalization properties of charged COPVs and their model compounds, as studied by Raman spectroscopy complemented by UV−vis−NIR spectroscopy, EPR spectroscopy, and quantum-chemical calculations. In addition to already reported **COPV1**−**6**, we studied the quinoidal molecules **Q(COPV*n*)** (n = 1, 2), which also have been prepared previously. The **Q(COPV*n*)**s serve not only as isoelectronic models of dicationic **COPV*n*** (Schemes 1 and 2) in their neutral states, but also as those of monocationic COPVs upon reduction, allowing delocalization of the extra negative charge to afford a mixed valence system. We newly synthesized **DA(COPV2)** (Scheme 2) to study the electronic communication between two end amino substituents, which also afforded a mixed valence system in its stable radical cationic state, similar to the radical anion of **Q(COPV2)**. We also synthesized a partially unbridged **B-COPV3** to evaluate the ring strain effect.

Scheme 2. Chemical Structures of Quinoidal COPV Derivatives Possessing Electron-Accepting Groups (Q(COPV1) and Q(COPV2)) as Models of Dicationic Species, Together with the Partially Unbridged COPV3 (B-COPV3) and the Symmetrically Substituted COPVs Possessing Electron-Donating Diphenyl Amino Groups (DA(COPV2))[a]

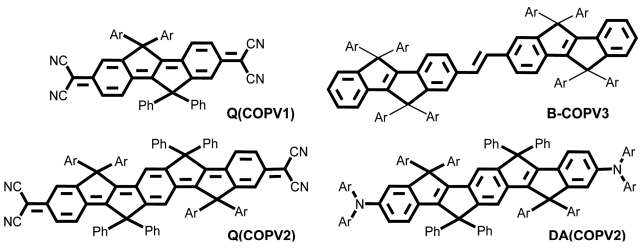

[a]Ar = 4-octylphenyl, Ph = phenyl.

Raman spectroscopy has long served as an invaluable tool for studies of conducting and conjugated polymers.[9,10] The changes in the band frequencies for the few Raman active normal modes in the vibrational spectrum of a conjugated system contain information relevant to electron−electron correlation and electron−nuclear couplings in a given molecular geometry.[11,12] The study on neutral **COPV*n*** reported previously is an example:[5] Raman frequencies of the ν(C=C)$_{vinyl}$ mode (red in Figure 1) and the coupled ν(C=C)$_{vinyl}$ + ν(CC)$_{phenyl}$ mode (blue in Figure 1) in the COPVs are sensitive to the molecular length, unlike those of the ordinary (unbridged) OPV (see Figure S1, Supporting Information for the Raman spectra of two OPV compounds of equivalent size to **COPV2** and **COPV4**) suggesting electron delocalization over the rigid planar COPV. On the other hand, strong electron pinning is suggested by the dihedral angle motions around the single bonds in OPVs.[11−13] Noteworthy is that the progressive frequency change of these stretching Raman bands is not continuous over the whole range of **COPV1** to **COPV6** but shows a gap upon going from **COPV2** to **COPV3** (Figure 1 right panel, red and blue marks), which is attributed to the significant release of the bicyclo[3.3.0]octene strain together with the concomitant relaxation of the bond length alternation pattern (Figure S2, Supporting Information).

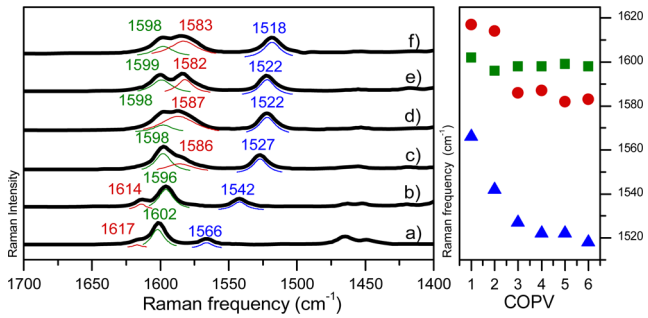

Figure 1. FT-Raman spectra of **COPV*n***. (left) Solid-state 1064 nm FT-Raman spectra of neutral **COPV*n***: (a) **COPV1**, (b) **COPV2**, (c) **COPV3**, (d) **COPV4**, (e) **COPV5**, and (f) **COPV6**. (right) COPV-size dependence of the frequency for the three most relevant Raman bands: ν(C=C)$_{vinyl}$ in red, ν(C=C)$_{phenyl}$ in green, and ν(C=C)$_{phenyl}$ + ν(C=C)$_{vinyl}$ in blue. The frequencies of the experimental spectra have been assigned by deconvolution. See Figure S3 and Table S1 of Supporting Information for vibrational eigenvectors of 1470−1440 cm^{-1} bands in **COPV1**.

EXPERIMENTAL AND THEORETICAL DETAILS

Synthesis. The preparation of the **COPV*n*** compounds and **Q(COPV1)** and **Q(COPV2)** has been reported previously.[14] The synthesis and characterization of **DA(COPV2)** and **B-COPV3** are described in detail in the Supporting Information. Chemical oxidations were carried out using 10^{-4} M solutions of the compounds in dry freshly distilled CH_2Cl_2 by stepwise addition of 10^{-4} M $FeCl_3$ or Et_3OSbCl_6 in CH_2Cl_2. Chemical oxidations were monitored in situ by UV−vis−NIR electronic absorption spectroscopy using a Cary 5000 UV−vis−NIR spectrometer from Varian. See Figures S4 and S5 in Supporting Information.

Raman Spectroscopy. The Raman spectra were recorded in resonance conditions by using the 1064, 785, or 532 nm excitations. In the UV−vis−NIR spectra of the oxidized compounds in Figures S4 and S5, Supporting Information, we show the Raman excitation used for their detection. The 1064 nm FT-Raman spectra were obtained with an FT-Raman accessory kit (FRA/106-S) of a Bruker Equinox 55 FT-IR interferometer. A continuous-wave Nd−YAG laser operating at

DOI: 10.1021/ja5125463
J. Am. Chem. Soc. 2015, 137, 3834−3843

1064 nm was employed for excitation. A germanium detector operating at liquid nitrogen temperature was used. Raman scattering radiation was collected in a backscattering configuration with a standard spectral resolution of 4 cm^{-1}. A total of 1000−3000 scans were averaged for each spectrum. Raman spectra with 785 nm excitation were collected using the 1 × 1 camera of a Bruker Senterra Raman microscope by averaging spectra during 50 min with a resolution of 3−5 cm^{-1}. A CCD camera operating at −50 °C was used. All spectra have been deconvoluted into Lorentzian shape bands to assign all of the components. Numerical data for each deconvoluted spectrum are shown at the end of the Supporting Information file.

Theoretical Calculations. Quantum-chemical calculations were performed in the framework of density functional theory[15] as implemented in the Gaussian 09 package.[16] Simulations were performed in the gas phase. The B3LYP exchange-correlational functional[17] and the 6-31G** basis set[18] were used in all calculations, except for NICS calculations, where 6-311+G(2d,p) basis set was used.

Instead of the real molecules, we studied model molecules lacking the aryl substituents (denoted by **-T** as for **COPV3-T** in Scheme 3) for theoretical simplicity (See section 6 of Supporting Information for a detailed explanation). The optimized structure of **B-COPV3-T** was planar at the B3LYP/6-31G** level. In addition, **Me_2-B-COPV3-T** was built as a model of **B-COPV3-T** with the central vinylene bond dimethylated to evaluate the substitutional effect on the central vinylene regarding the theoretical Raman frequencies. Theoretical frequencies were scaled uniformly by a scale factor of 0.96. All vibrational normal modes associated with the relevant theoretical frequencies are provided in the Supporting Information. The unrestricted (U)B3LYP/6-31G** approach was used for the open-shell radical cation and dications. To simulate the open-shell ground-state structures of the dication, we used the broken-symmetry option with the guess=mix keyword along with unrestricted wave functions at the (U)B3LYP level.

Scheme 3. Chemical Structures of the Three Model Compounds of COPV3 Together with the Relevant Theoretical Parameters from the DFT/UB3LYP/6-31G Calculations**

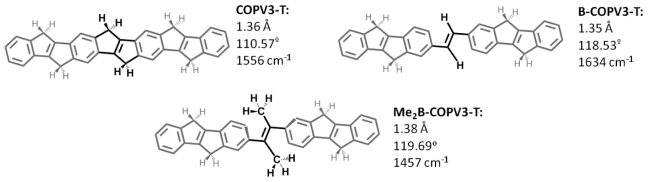

RESULTS AND DISCUSSION

Neutral COPV*n* Compounds: Ring Strain and Raman Frequencies. We start by describing the neutral species to first assess the effects of ring strain of the bicyclo[3.3.0]octene group. Figure 2 shows the theoretical Raman spectra of model compounds (**COPV3-T** and **B-COPV3-T** for the left panel of Figure 2a,c) and the experimental Raman spectra of **COPV3** and **B-COPV3** (left panel of Figure 2b,d). The C−C stretching of the phenyl rings ($\nu(CC)_{phenyl}$) and that of the vinyl C=C bonds ($\nu(C{=}C)_{vinyl}$) are colored in green and red, respectively. The spectra show good correlation between experimental and theoretical data. Thus, the theoretical band at 1589 and 1585 cm^{-1} (green) in **COPV3-T** and **B-COPV3-T**, respectively, can be assigned to the $\nu(CC)_{phenyl}$ mode (see Table S2, Supporting Information, for the vibrational eigenvector) and correspond to the experimental band at 1598 and 1596 cm^{-1} in **COPV3** and **B-COPV3**, respectively. On the other hand, the theoretical band at 1556 cm^{-1} in **COPV3-T** (red) is assigned to the $\nu(C{=}C)_{vinyl}$ mode, mostly of the central one (Table S2, Supporting Information), that upshifts to 1629 cm^{-1} in **B-COPV3-T** and that are observed in the experimental spectra at 1586 cm^{-1} in **COPV3** and at 1634 cm^{-1} in **B-COPV3**.

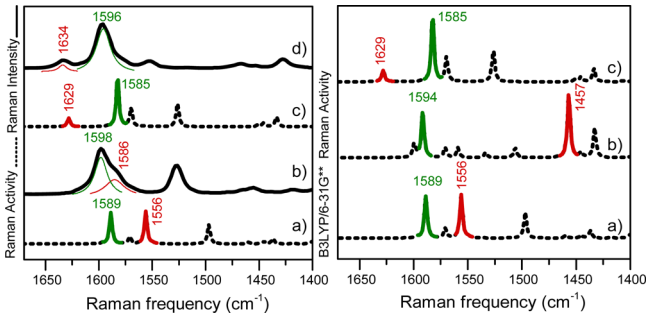

Figure 2. Experimental Raman spectra of **COPV3** and **B-COPV3**, together with theoretical B3LYP/6-31G** predictions of their model compounds **COPV3-T** and **B-COPV3-T**. $\nu(C{=}C)_{vinyl}$ and $\nu(C{=}C)_{phenyl}$ bands are colored in red and green, respectively. (left) Theoretical spectra of (a) **COPV3-T** and (c) **B-COPV3-T** and experimental FT-Raman spectra of (b) **COPV3** and (d) **B-COPV3**. (right) Theoretical spectra of (a) **COPV3-T** (b) **Me_2-B-COPV3-T**, and (c) **B-COPV3-T**. The experimental frequencies have been assigned by deconvolution.

This upshift of the vinylene mode frequency (1585 →1634 cm^{-1}) upon removal of the bridge from **COPV3** to **B-COPV3**, and hence the ring strain, may appear counterintuitive at a first glance and might be understood as due to the increase of the s-character of the vinylene bond in the partially unstrained compound as a result of releasing it from the bicyclo[3.3.0]-octene framework (the C=C−C(H) angle changes from 110.57° in **COPV3-T** to 118.53° in **B-COPV3-T** in Scheme 3). The absence of σ–π hyperconjugation between the vinylene and the C(bridging)−C(ipso Ar) σ bonds on **COPV3** → **B-COPV3** can also contribute to the frequency upshift.

However, from **COPV3-T** to **B-COPV3-T**, the substitution pattern of the central vinylene is altered from tetra-substituted to disubstituted, and this might have an influence on the Raman frequencies. To clarify this, we have calculated the Raman spectrum in a **Me_2-B-COPV3-T** tetra-substituted unstrained model, and now the $\nu(C{=}C)_{vinyl}$ band appears downshifted to 1457 cm^{-1} (right panel Figure 2b, see Table S2, Supporting Information, for the vibrational eigenvector). This indicates that although the s-character of the C=C of **Me_2-B-COPV3-T** presumably increases, its liberation from the bicyclo[3.3.0]-octene strain provokes a overall downshift of the associated Raman band frequency, which is much more physically intuitive because a more released bond needs less energy to be stretched. Note that the $\nu(CC)_{phenyl}$ mode in this model compound, again, remains almost unchanged (predicted at 1594 cm^{-1}) (See Figure S9, Supporting Information, for a detailed explanation). A similar trend was also observed for the Raman spectra of *trans*-stilbene (**OPV1**) in comparison with the smallest **COPV1** in Figure S10 and Table S3, Supporting Information.

Radical Cations of COPV*n*. This section describes the Raman spectra of the radical cations of the parent COPVs, $[\mathbf{COPV}n]^{\bullet+}$, and the isoelectronic monovalent species of substituted COPVs ($[\mathbf{DA(COPV2)}]^{\bullet+}$ and $[\mathbf{Q(COPV2)}]^{\bullet-}$). The former were found to possess confined radical cation character, whereas the latter show fully delocalized mixed valence systems. The difference between the parent and the substituted COPVs is discussed below.

DOI: 10.1021/ja5125463
J. Am. Chem. Soc. 2015, 137, 3834−3843

Raman Spectra of the COPV Radical Cations. The spectra of the radical cations [**COPV*n***]$^{\bullet+}$ in Figure 3 present important

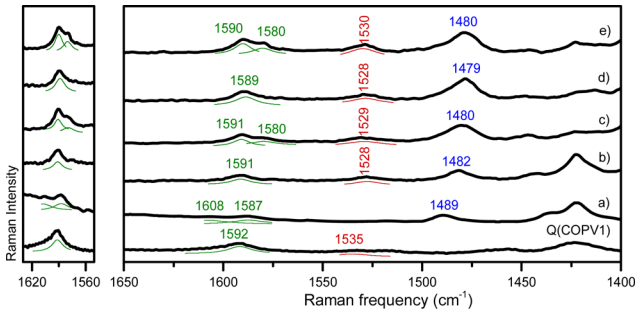

Figure 3. Resonant Raman spectra of the radical cation species of COPVs: (a) [**COPV2**]$^{\bullet+}$, (b) [**COPV3**]$^{\bullet+}$, (c) [**COPV4**]$^{\bullet+}$, (d) [**COPV5**]$^{\bullet+}$, and (f) [**COPV6**]$^{\bullet+}$ together with the Raman spectrum of **Q(COPV1)**. ν(CC)$_{phenyl}$ and ν(C=C)$_{vinyl}$ bands in green and red, respectively. The experimental frequencies have been assigned by deconvolution.

trends: (1) The Raman spectra of the radical cations show significant downshifts upon oxidation regarding the neutrals. (2) The Raman peak positions of these monocationic species are almost insensitive to the molecular length of the COPV molecule, in contrast to those of the neutral molecules. With the help of the DFT/UB3LYP/6-31G** calculations, we can assign the main peaks to ν(CC)$_{phenyl}$ (1580−1590 cm^{-1}, green), ν(C=C)$_{vinyl}$ (ca. 1530 cm^{-1}, red), and the coupled ν(C=C)$_{vinyl}$ + ν(CC)$_{phenyl}$ (blue) (see Table S4, Figure S11, Supporting Information).

The first trend can be readily seen in the ν(C=C)$_{vinyl}$ and the coupled ν(C=C)$_{vinyl}$ + ν(CC)$_{phenyl}$ bands, which show significant downshifts by 50−80 cm^{-1}, while the ν(CC)$_{phenyl}$ bands shift down only by 10−15 cm^{-1}. We also noticed the similarity between [**COPV*n***]$^{\bullet+}$ and **Q(COPV1)** (Scheme 2, bottom, for the chemical structure and Figure S12 and Table S5, Supporting Information, for the assignment of the main Raman bands).[19] The latter has a well-defined quinoidal structure for the benzene rings and a vinylene moiety with a much reduced double-bond character.[14] The resemblance between the [**COPV*n***]$^{\bullet+}$ spectra and that of **Q(COPV1)** supports the quinoidization of the benzenes and the C=C → C−C vinylene transformation upon one-electron oxidation of **COPV*n*** and corroborates the greater sensitivity of the vinylene bonds to the strain and the overall π-conjugation. This agrees well with the trend in the neutral species, as discussed already for **COPV3-T**, **B-COPV3-T**, and **Me$_2$-B-COPV3-T**. The increase in the overall π-conjugation within the oxidized segment also contributes to the frequency change in the ν(C=C)$_{vinyl}$ band, as shown by the changes in the benzene frequencies as a result of quinoidization (see the change from **COPV1** to **Q(COPV1)**). According to the convention in the physics of conducting polymers, we see this as the formation of a *polaron-like* charge defect in the phenylene−vinylene skeleton.

The second trend suggests that structural relaxation is maximal in the quinoidal segments, although the charge defect does not cover the whole π-electron framework because of the cost of breaking the aromaticity of all rings. This cost results in the confinement of the radical cation within the central part of the molecule. Particular insights can be drawn from the aspect of the ν(CC)$_{phenyl}$ bands at 1580−1590 cm^{-1}: they appear as single peaks in [**COPV3**]$^{\bullet+}$ and [**COPV5**]$^{\bullet+}$, while they can be described as double peaks for [**COPV4**]$^{\bullet+}$ and [**COPV6**]$^{\bullet+}$. Assuming confined polaron character, this even−odd effect can be addressed by considering that [**COPV3**]$^{\bullet+}$ and [**COPV5**]$^{\bullet+}$ have a vinylene bond in the center of the molecule flanked by two symmetrically equivalent benzene rings on which the radical cation is delocalized. In the case of [**COPV4**]$^{\bullet+}$ and [**COPV6**]$^{\bullet+}$, a strongly quinoidalized benzene ring occupies the center of the molecule and is responsible for the large downshifted band at ∼1580 cm^{-1}, while the band at ∼1590 cm^{-1} is due to the two symmetric phenyl rings next to the central ring. These two benzene rings obviously have less pronounced quinoidal character. Thus, the radical cation in [**COPV6**]$^{\bullet+}$ extends over three phenyl moieties, including seven consecutive fused planar rings (see Figure S13, Supporting Information, for the chemical structures). Such extraordinarily large extension of a charge defect (charge delocalization) is impossible in conventional flexible phenylene−vinylene compounds.[11,12] The structural and electronic uniqueness of the planar constrained COPVs is amply illustrated here for [**COPV6**]$^{\bullet+}$.

*Radical Cations of COPV and Mixed Valence Systems of **COPV2**.* The radical cation and the anion species of [**DA(COPV2)**]$^{\bullet+}$ and [**Q(COPV2)**]$^{\bullet-}$, having electron-donating and -accepting diphenylamino and dicyanomethylene groups, respectively, represent systems where a positive and a negative charge is fully delocalized between the two terminal groups to form class III mixed valence states (see discussion of the intervalence charge transfer bands in Figure S14, Supporting Information). Thus, they are different from unsubstituted [**COPV*n***]$^{\bullet+}$, where the radical cation is confined within the molecular center.

This section of the present study is therefore related to the electron transfer (ET) through the COPV molecular wire; the ET occurs exclusively by a tunneling mechanism.[8] Note that the ET through a molecular wire may occur via either tunneling or hopping depending on the structure of the wire;[7,20] the ET through OPV occurs by a hopping mechanism mediated by low-frequency conformational torsional modes.[3] In light of the charge confinement in the parent COPV discussed above, the presence or absence of electronic communication between the two terminal substituents via the COPV bridge in **DA-(COPV2)** and **Q(COPV2)** emerges as an intriguing subject of the present study. The Raman fingerprints of these substituted COPVs were found to play an important role.[21]

In the radical cation state, [**DA(COPV2)**]$^{\bullet+}$ can behave as a mixed valence system[22] because it possesses two identical electron-donating groups that stabilize the positive charge on the **COPV2** moiety (see Scheme 4). Given the large electron-donating capacity of the amino groups, in the radical cation state, one would expect the positive charge to be placed either in or around one of the two amino groups (localized or class II mixed valence system[22]) or fully delocalized between the two amino groups through the **COPV2** bridge (delocalized or class III mixed valence system[22]). The same consideration is valid for the distribution of the negative charge of the radical anion [**Q(COPV2)**]$^{\bullet-}$.

The deconvoluted Raman spectrum of [**DA(COPV2)**]$^{\bullet+}$ suggests the presence of two types of quinoidal rings in [**DA(COPV2)**]$^{\bullet+}$, which is different from that of [**COPV2**]$^{\bullet+}$ in that the main band is at a lower frequency (1578 cm^{-1}) and is accompanied by an additional weaker peak at 1589 cm^{-1} (Figure 4). The Raman profile of the [**Q(COPV2)**]$^{\bullet-}$ radical anion also has two main bands at 1584 and 1601 cm^{-1}, which,

DOI: 10.1021/ja5125463
J. Am. Chem. Soc. 2015, 137, 3834−3843

Scheme 4. Chemical Structures after Oxidation and Reduction of DA(COPV2) and Q(COPV2), Respectively

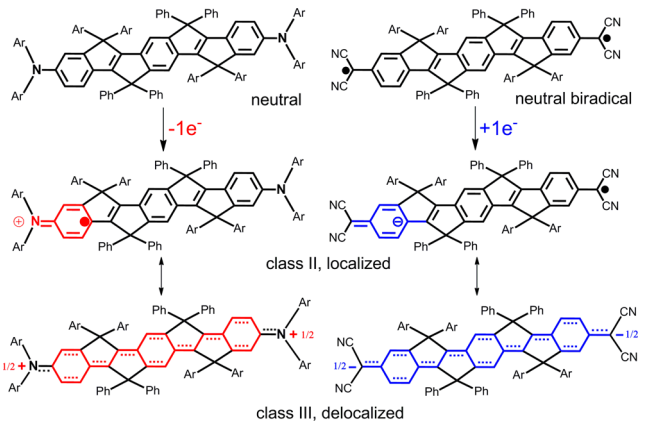

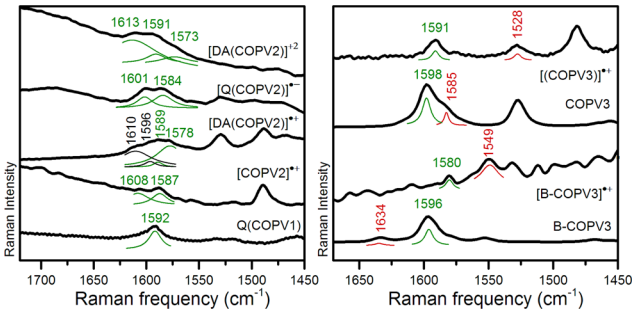

Figure 4. Resonant Raman spectra of the radical cation and dication species of **DA(COPV2)**, radical anion of **Q(COPV2)**, and radical cation of **[B-COPV3]**$^{\bullet+}$. $\nu(CC)_{phenyl}$ and $\nu(C{=}C)_{vinyl}$ are shown in green and red, respectively. The frequencies of the experimental spectra have been assigned by deconvolution.

interestingly, appear in a region similar to the region found in the neutral **Q(COPV2)** compound (Figure 3, bottom). Given that the structure of neutral **Q(COPV2)** is only partially quinoidal (see the next section), it seems that the structure of its anion also remains partially quinoidal, which explains the similarity to the spectrum of **[DA(COPV2)]**$^{\bullet+}$, which has a pseudoquinoidal structure. The resemblance of the vibrational Raman spectra of **[DA(COPV2)]**$^{\bullet+}$ and **[Q(COPV2)]**$^{\bullet-}$ in terms of a double band pattern for their $\nu(CC)_{phenyl}$ modes suggests the presence of two different benzene rings mainly involved in the stabilization of the injected charge, which stands in contrast to the simpler Raman pattern of the unsubstituted **[COPV2]**$^{\bullet+}$ (Figure 4a).

The formation of class III mixed valence states in these substituted COPVs has been unknown for a fully organic phenylenevinylene system and is fully consistent with the charge stabilization of the strongly electron-donating and -accepting ability of diphenylamino and dicyanomethylene groups. That is, a driving force originated from the electronic coupling between the two diphenylamino or dicyanomethylene groups can surpass the aromaticity stabilization to yield fully charge-delocalized monovalent structures, as opposed to the confined character of the charge defect in **[COPV2]**$^{\bullet+}$. One may argue that the electronic coupling between the external donors or acceptors is enhanced by the planarity of the bridge and by the ring strain, which produces small reorganization energies toward the formation of extended fully delocalized quinoidal structures.

The carbon-bridging effect in COPVs was also shown by the Raman spectrum of the radical cation of **[B-COPV3]**$^{\bullet+}$, which displays a very strong Raman band at 1549 cm^{-1} (Figure 4). In accordance with previous studies on unbridged (nonfused) thiophene−vinylene compounds,[23] this band can be assigned to the unbridged $\nu(C{=}C)_{vinyl}$ mode, which undergoes a significant frequency downshift upon oxidation. From a structural point of view, this suggests that the charge defect is centered largely at the vinylene moiety with a moderate influence of the lateral **COPV1** units. This shows the significance of the COPV bridging and planarization of the conjugated backbone for the stabilization and π-electron delocalization of the injected charges. Pinning or confinement of the extra charge in OPV oligomers has been well described elsewhere.[6,8]

Dications of COPV*n*. Raman spectroscopy of the dicationic species provided interesting insight on the spin−spin coupling (double spin polarization) within the fully planar π-conjugated framework. First, for the sake of comparison, we describe the properties of the neutral tetracyano-substituted quinoidal COPV compounds, **Q(COPV1)** and **Q(COPV2)** in Scheme 2, with the latter having the same core as **COPV2**. We then analyze the Raman spectra of the divalent dications in terms of their biradicaloid character. This kind of Kekulé-type biradicals is now being intensively studied given their relevant electronic and photonic properties with potential applications in areas such as spintronics, photovoltaics, and energy storage.[24−27]

Raman Spectra of Tetracyano-Substituted COPV Compounds. Figure 5 shows the Raman spectra of the tetracyano-

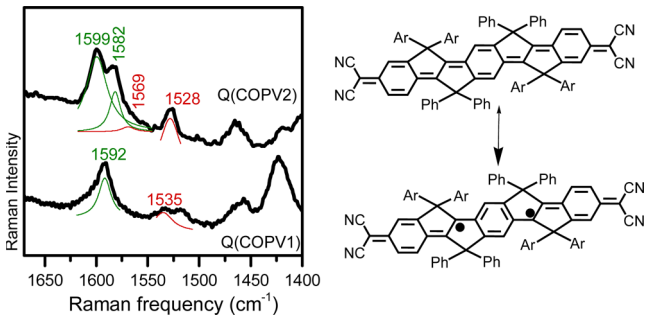

Figure 5. (left) Resonant Raman spectra of **Q(COPV1)** and **Q(COPV2)**. $\nu(CC)_{phenyl}$ and $\nu(C{=}C)_{vinyl}$ bands are shown in green and red, respectively. The frequencies of the experimental spectra have been assigned by deconvolution. (right) Biradical transformation of **Q(COPV2)** according to (U)B3LYP/6-31G**.

methylene-substituted **Q(COPV1)** and **Q(COPV2)** compounds. **Q(COPV1)** has a closed-shell quinoidal structure,[14] and as such it was discussed in the above radical cation section. In contrast, the ground electronic state of **Q(COPV2)** is an open-shell aromatic shape in accordance with a Kekulé-type biradical representation.[14] Such biradicals can be seen as a ground electronic state of singlet multiplicity (see Scheme 4 and Figure 5) with the parent triplet state at a slightly higher energy, a situation that violates Hund's rule and that arises as a result of the mechanism of double-spin polarization (DSP)[28,29] (see the following sections). Now, we discuss the process of formation of the aromatic biradical species from the starting quinoidal structures going from **Q(COPV1)** to **Q(COPV2)**: whereas **Q(COPV1)** keeps the two benzene rings mostly quinoidal, the energy gained by total or partial aromatization of the rings in **Q(COPV2)** exceeds the energy required to break a

DOI: 10.1021/ja5125463
J. Am. Chem. Soc. 2015, 137, 3834−3843

double bond, allowing the formation of a biradical. In addition, part of the energy gained by aromatization in the formation of the biradical is consumed by the recovery of bicyclo[3.3.0]-octene strain in the aromatic form, which is an intrinsic property of the COPV cores.

The difference between the closed- and open-shell characters of **Q(COPV1)** and **Q(COPV2)** are next clarified by Raman spectra. As already seen in the radical cations, the band at 1592 cm^{-1} of **Q(COPV1)** is due to the $\nu(CC)_{phenyl}$ modes of the two symmetric quinoidal benzenes, which together with the bands around 1530 cm^{-1} of the $\nu(C{=}C)_{vinyl}$ mode produce the pair of relevant vibrational bands of a full quinoidal pattern (Figure S14 and Table S5, Supporting Information). In **Q(COPV2)**, the $\nu(CC)_{phenyl}$ mode evolves into the 1599 and 1582 cm^{-1} doublet, the former associated with the central benzene ring that displays an aromatic-like structure embodying the biradical species and the latter due to the other $\nu(CC)_{phenyl}$ mode from the outermost quinoidal-like rings (see scheme in Figure 5). A new signal is detected on the low-frequency side of this $\nu(CC)_{phenyl}$ doublet, at 1569 cm^{-1}, which together with the 1528 cm^{-1} band represent the two related $\nu(C{=}C)_{vinyl}$ modes of the aromatic and quinoidal parts, respectively.

Therefore, being similar to the case of neutral COPVs, the bands are grouped in pairs, 1599/1569 cm^{-1} and 1582/1528 cm^{-1} for the $\nu(CC)_{phenyl}/\nu(C{=}C)_{vinyl}$ bands of the aromatic-like and quinoidal-like parts of the biradical, respectively. In terms of the most intense Raman bands, the fingerprint of the formation of the biradical species from a quinoidal structure is easily detected by the change of the single $\nu(CC)_{phenyl}$ peak at 1592 cm^{-1} in **Q(COPV1)** into the double peaks at 1599/1582 cm^{-1} in **Q(COPV2)**.

Raman Spectra of COPV Dications. Figure 6 shows the Raman spectra of the dicationic species of the COPV compounds.

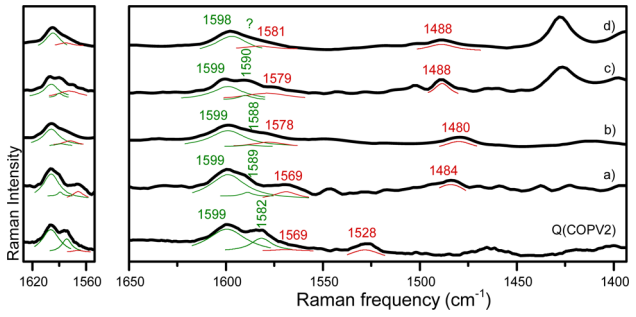

Figure 6. Resonant Raman spectra of the stable dicationic species of the COPV compounds: (a) $[\mathbf{COPV3}]^{2+}$, (b) $[\mathbf{COPV4}]^{2+}$, (c) $[\mathbf{COPV5}]^{2+}$, and (d) $[\mathbf{COPV6}]^{2+}$ together with that of the neutral biradical **Q(COPV2)**. $\nu(CC)_{phenyl}$ and $\nu(C{=}C)_{vinyl}$ bands are shown in green and red, respectively. The frequencies of the experimental spectra have been assigned by deconvolution.

The notable resemblance between the spectra of the COPV dications and that of **Q(COPV2)** provides an important insight into the electronic structure of the dications. We noticed that the peak positions of the 1580–1600 cm^{-1} bands are rather insensitive to the size of the oligomer. One therefore expects that one-electron oxidation of the radical cations to the dications produces a further increment in the quinoidal structure from the center of the molecule toward the molecular ends as a result of electrostatic repulsion between the two positive charges. In this way, a superbenzoquinoidal sequence from one extreme to the other forms, or alternatively a *bipolaron-like* structure with a characteristic closed-shell singlet ground electronic state (see Scheme 5).

Scheme 5. Closed-Shell Quinoidal and Open-Shell Aromatic Singlet Resonance forms of $[\mathbf{COPV6}]^{2+}$

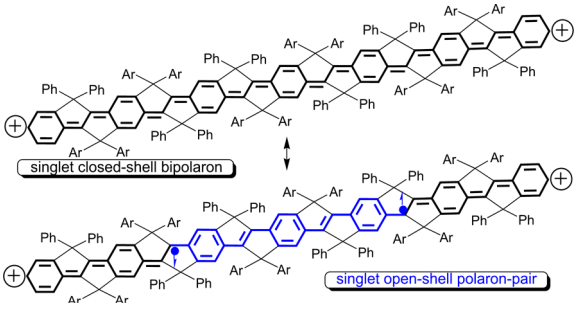

According to that described for **Q(COPV2)**, at a given chain size, this full quinoidal bipolaron form is inherently unstable and will eventually undergo an aromatization recovery by breaking one of the highly conjugated double bonds to afford a dicationic biradical species, or biradical *polaron-pair* (see Scheme 5). An identical situation has been described in oligothiophene dications.[23] The formation of this biradical dicationic species would nicely justify the resemblance between the Raman spectra of neutral **Q(COPV2)** and of the divalent dications and the evolution of the Raman spectra from the COPV radical cations to the COPV dications, which follows the same tendency as was described in **Q(COPV1)** → **Q(COPV2)** and is assigned as the Raman spectroscopic fingerprint of the quinoidal → biradical transformation, in such ways as 1591 → (1599, 1589) cm^{-1} for $[\mathbf{COPV3}]^{\bullet+}$ → $[\mathbf{COPV3}]^{2+}$, 1591 (1580) → (1599, 1588) cm^{-1} for $[\mathbf{COPV4}]^{\bullet+}$ → $[\mathbf{COPV4}]^{2+}$, 1589 → (1599, 1590) cm^{-1} for $[\mathbf{COPV5}]^{\bullet+}$ → $[\mathbf{COPV5}]^{2+}$, and 1590 (1580) → (1597, 1585–1590) cm^{-1} for $[\mathbf{COPV6}]^{\bullet+}$ → $[\mathbf{COPV6}]^{2+}$. The $\nu(C{=}C)_{vinyl}$ modes of the innermost biradical aromatic parts might be associated with the bands at 1569, 1578, 1579, and 1581 cm^{-1} for $[\mathbf{COPV3}]^{2+}$, $[\mathbf{COPV4}]^{2+}$, $[\mathbf{COPV5}]^{2+}$, and $[\mathbf{COPV6}]^{2+}$, respectively. Those $\nu(C{=}C)_{vinyl}$ modes of the external biradical quinoidal parts appear as broad bands below 1500 cm^{-1}: 1484, 1480, 1488, and 1488 cm^{-1}, respectively, from $[\mathbf{COPV3}]^{2+}$ to $[\mathbf{COPV6}]^{2+}$. These assignments are also supported by the theoretical calculations on $[\mathbf{COPV4}]^{2+}$ and $[\mathbf{COPV6}]^{2+}$ as representative examples (see Figure S15, Supporting Information).

The most intense bands around 1600 cm^{-1} emerging from $\nu(CC)_{phenyl}$ of the aromatic benzenes placed in the central part of the molecules between the radical centers of the open-shell singlet (see Scheme 4) are now discussed in more detail. These peaks scarcely change in their frequencies, in accordance with the strong electron pinning in the benzene rings because of their aromaticity, an effect that is reinforced in the dications by their strongly electron-deficient nature. The frequencies of the weak bands between 1570 and 1585 cm^{-1} already assigned to the $\nu(C{=}C)_{vinyl}$ modes are typical of bicyclo[3.3.0]octene moieties, which to a large extent have recovered their strain character revealing their placement in the molecular fragment between the aromatic benzenes in the interradical moiety.[5]

Between these $\nu(CC)_{phenyl}$ and $\nu(C{=}C)_{vinyl}$ aromatic features, additional bands around 1590 cm^{-1} are detected, largely overlapped with the two above but resolved by spectral deconvolution. On the basis of their frequency values and in

DOI: 10.1021/ja5125463
J. Am. Chem. Soc. 2015, 137, 3834–3843

connection with the assignment in **Q(COPV2)**, these new bands might be associated with $\nu(CC)_{phenyl}$ modes of benzoquinoidal structures ascribed to those rings at the outermost molecular parts. Finally, below 1500 cm^{-1}, we observe the $\nu(C{=}C)_{vinyl}$ modes of these quinoidal outermost sites. This spectroscopic description provides a full picture of the dication biradicals consisting of the coexistence of a strained aromatic fragment in the middle, placed between the two unpaired electrons, flanked by two quinoidal structures between the unpaired electrons and the positive charges at the termini.

Theoretical calculations at the (U)B3LYP/6-31G** level also suggest a crossover from closed-shell character of dicationic COPVs to open-shell upon elongation of the molecular length. Figure 7 shows the energy differences

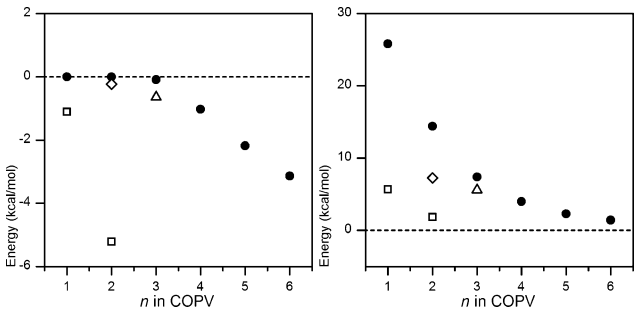

Figure 7. DFT (U)B3LYP/6-31G** energy differences for the COPV dications: Singlet open-shell minus the singlet closed-shell energies (left) and triplet minus singlet open-shell energies (right). Black circles for $[\mathbf{COPV}n\mathbf{\text{-}T}]^{2+}$, squares for $[\mathbf{Q(COPV1)\text{-}T}]$ and $[\mathbf{Q(COPV2)\text{-}T}]$, rhombus for $[\mathbf{DA(COPV2)\text{-}T}]^{2+}$, and triangles for $[\mathbf{B\text{-}COPV3\text{-}T}]^{2+}$.

between the open-shell and closed-shell singlet and triplet configurations of the COPV dications calculated at the (U)B3LYP/6-31G** level of theory. For the shorter dications, $[\mathbf{COPV1\text{-}T}]^{2+}$ and $[\mathbf{COPV2\text{-}T}]^{2+}$, the closed-shell singlet quinoidal form is the most stable. In $[\mathbf{COPV3\text{-}T}]^{2+}$, however, the open-shell biradical singlet becomes slightly preferred, a stabilization that continuously increases for the longer dications. These theoretical data are in excellent agreement with the titration experiments for **COPV6** that have been conducted up to the dication and followed by EPR spectroscopy (see Figure S16, Supporting Information). Once the $[\mathbf{COPV6}]^{2+}$ is generated by a stoichiometric amount of $THI^{\bullet+}ClO_4$, the EPR signal does not completely disappear at room temperature, suggesting the persistence of a magnetically active species inherently associated with the dication. Upon heating the solution of the dication, the intensity of the EPR signal increases and then decreases upon cooling.

The temperature-dependent EPR data were fitted to the Bleaney–Bowers equation from which the singlet–triplet gap is experimentally deduced to be 1.7 kcal/mol, which nicely coincides with that theoretically predicted from the (U)-B3LYP/6-31G** calculations for the singlet–triplet gap of $[\mathbf{COPV6\text{-}T}]^{2+}$ of 1.4 kcal/mol (Figure 7). The theoretical analysis also supports the fact that the Raman spectroscopic behaviors of $[\mathbf{COPV3\text{-}T}]^{2+}$ and longer represent the biradical aromatic form in the ground electronic state. While EPR spectroscopy shows the formation of the triplet biradical species, Raman spectroscopy is unique in providing complementary information on molecular structure.

Raman Spectra and DSP. The stabilization of these quinoidal extremities in the **COPV** biradical dications can be explained by DSP,[28] which accounts for the π-conjugation or π-delocalization of the two paired electrons in the highest doubly occupied molecular orbital (HOMO) over the two singly occupied molecular orbitals (SOMOs).[30] In Kekulé biradicals, DSP is additive for the singlet and competitive for the triplet, meaning that the singlet biradical has two possible stabilizing contributions because there is no restriction for the spin delocalization (Scheme 6a, see ref 30). However, for the triplet, because both unpaired electrons have the same spin sign, only one stabilization contribution is possible (see red arrow in Scheme 6).

Scheme 6. Theoretical Pictures of the Dication of COPV2[a]

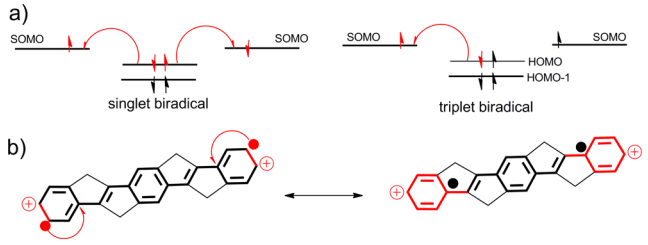

[a](a) Molecular orbital visualization of the DSP effect with double conjugation in the singlet biradical and single conjugation in the triplet (see ref 30). (b) Valence bond visualization of the conjugation effect of the unpaired electrons of the biradical.

This interpretation is in good agreement with the previous energy calculations, which always place the triplet dicationic state at higher energies than the singlet biradical dication (see Figure 7), with the singlet–triplet energy gap, ΔE_{ST}, being a measure of the magnitude of the DSP effect. In fact, ΔE_{ST} decreases as the molecular size increases, which provides information on the specific DSP action at the terminal moieties (see red rings in Scheme 6b). In such, the delocalization of the unpaired electrons with the bridge by DSP produces a partial quinoidization at the terminal sites, as revealed by the Raman assignment of the "benzoquinoidal" bands around 1590 cm^{-1}, in addition to the built-in ring strain within the COPV structure that stabilizes the quinoidal form as well.

Electronic and structural effects on DSP were clarified by the measurements on the COPV derivatives $[\mathbf{DA(COPV2)}]^{2+}$ and $[\mathbf{B\text{-}COPV3}]^{2+}$. The Raman spectrum of $[\mathbf{DA(COPV2)}]^{2+}$ shows the two characteristic bands at 1613 and 1591 cm^{-1} that evolve from those at 1589 and 1578 cm^{-1} in $[\mathbf{DA\text{-}(COPV2)}]^{\bullet+}$. The frequency upshift can be an indication of the generation of a biradical for this dication in accordance with the (U)B3LYP/6-31G** calculations in Figure 7, which predict that the open-shell form of $[\mathbf{DA(COPV2\text{-}T)}]^{2+}$ is slightly more stable than the closed-shell form.

The same (U)B3LYP/6-31G** calculations show that the ground electronic state of the dication species of $[\mathbf{B\text{-}COPV3\text{-}T}]^{2+}$ is also a singlet open shell (see Figure 7). However, in this dication, rotations around the central C–C bond are not restricted by which conjugation can be eventually broken allowing the collapse of DSP and consequently the stabilization of the triplet. Unfortunately, oxidation of the radical cation of **B-COPV3** up to its dication ($[\mathbf{B\text{-}COPV3}]^{\bullet+} \rightarrow [\mathbf{B\text{-}COPV3}]^{2+}$) affords an unstable species that could not be characterized by Raman spectroscopy, in agreement with the propensity to stabilize the more reactive triplet.

A Unified NICS View of the Electronic Structure. The electronic structures and in particular the degree of aromaticity

DOI: 10.1021/ja5125463
J. Am. Chem. Soc. 2015, 137, 3834–3843

Table 1. DFT (U)B3LYP/6-311+G(2d,p) NICS Values of Neutrals, Radical Cations, and Dications of COPV6-T and Neutral COPV2-T and Q(COPVn)-T as Well as the Radical Cation and Anion of DA(COPV2)-T and Q(COPV2)-T, Respectively, in Their Ground Electronic States

	ring number[a]					ring number[a]	
	4	3	2	1		2′	1′
COPV2-T			−8.955	−8.117	**Q(COPV1)-T**		−3.825
COPV6-T	−8.936	−7.958	−7.862	−7.856	**Q(COPV2)-T**	−5.781	−6.988
[**COPV6-T**]$^{\bullet+}$	−8.921	−7.121	−6.577	−6.465	[**DA(COPV2)-T**]$^{\bullet+}$	−6.644	−5.645
[**TCOPV6-T1**]$^{2+}$	−8.211	−5.472	−6.075	−6.806	[**Q(COPV2)-T**]$^{\bullet-}$	−5.990	−6.374

[a]

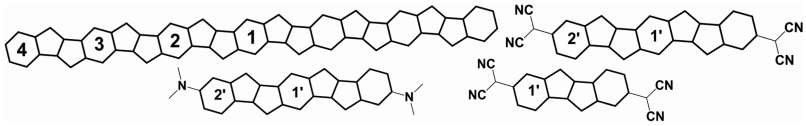

(quinoidization) of the phenyl rings can be complementarily evaluated with the aid of nucleus-independent chemical shift (NICS) analysis.[31] Table 1 summarizes the NICS values obtained at the DFT (U)B3LYP/6-311+G(2d,p) level of calculation for the phenyl rings of the **COPV6-T** model compound in the different oxidation levels and in the **Q(COPVn)-T** oligomers as well. Supporting Information provides all NICS data and discussion.

For the neutral molecules, NICS values of the benzene rings in the parent represent aromatic structure. For instance, in **COPV2-T**, these values are −8 and −9. For **Q(COPV1)-T**, the benzene ring has a NICS value of −3.8, representative of a well-defined quinoidal shape. In neutral **Q(COPV2)-T**, however, the NICS values are −6.9 in the central benzene ring and −5.7 in those at the terminals; hence the innermost ring is more aromatic than those connected to the dicyanomethylenes, revealing the formation of an open shell pseudoaromatic structure in the molecular center with the peripheral rings more quinoidized due to the effect of double spin polarization, which is consistent with the previous experimental study.[14]

For the radical cations, rings in the center have less negative NICS values characteristic of a quinoidal form whereas those at the outermost sites have aromatic character (i.e., −8.9 in [**COPV6-T**]$^{\bullet+}$). This shows that oxidation induces quinoidization in the molecular center and that the quinoidal character decreases as it goes to the external sites, which is in agreement with the Raman description of the polaron-like charge defect confined in the molecular center.

For the dications of COPV2, [**COPV2-T**]$^{2+}$ shows a NICS pattern characteristic of a well-defined quinoidal shape in the three rings, in accordance with a singlet closed shell structure similar to **Q(COPV1)-T**. In the largest molecule, [**COPV6-T**]$^{2+}$, the central ring has the more aromatic character (NICS value of −6.8), while the values increase toward the extremities (−6.07 and −5.4 for rings 2 and 3 in Table 1), highlighting a progressive quinoidization at the outermost sites. This trend is similar to the neutral **Q(COPV2)-T** and in agreement with the electronic configuration based on double spin polarization. The NICS value of ring number 4 in [**COPV6-T**]$^{2+}$ deviates from this tendency because of the absence of the coefficients in the terminal benzene rings in the relevant frontier orbitals (Kohn–Sham orbitals are shown in Figure S17, Supporting Information).

Finally, NICS values for the radical anion and cation of **Q(COPV2)-T** and **DA(COPV2)-T**, respectively, have been also included in Table 1. For [**DA(COPV2)-T**]$^{\bullet+}$, the NICS values of the two phenyl rings, −6.6 and −5.6, are much more similar than those in [**COPV2-T**]$^{\bullet+}$, −7.8 and −4.7, indicating the much more delocalized character of the charge structural defect on the whole COPV framework in line with a class III mixed valence species described in the previous sections. For [**Q(COPV2)-T**]$^{\bullet-}$, the two NICS values, −5.9 and −6.3, are similar to those of the neutral **Q(COPV2)-T** species, −5.7 and −6.9, revealing that injection of one additional electron does not affect much the original electronic structure, which already has a pseudoaromatic biradical character.

CONCLUSIONS

Raman spectroscopy of stable charged COPVs revealed the exceptional π-conjugation of these species deriving from the synergetic effects of ring planarization, fusion, and strain. The structures of their radical cations are benzo-quinoidal, and their formation is promoted by the release of ring strain of the bicyclo[3.3.0]octene moiety and impeded by the rupture of benzene aromaticity, resulting in charge defects confined in the molecular centers. The dications, in contrast, display recovery of aromaticity at the molecular center and the development of biradical character, which does not cover the whole molecule, either, because of the DSP and ring strain. COPV compounds possessing electron acceptors and electron donors afforded monovalent mixed-valence character that displays quite similar spectra and structures, in line with the fully delocalized electronic structure within the COPV moiety with fully quinoidal structure. These quinoidal cations, as a model of polarons, and these aromatic dications, as a model of polaron pairs, represent unprecedented forms for the charge defects in this class of π-conjugated *para*-phenylenevinylene compounds. Detailed studies of molecular phenomena occurring in these molecular systems are forthcoming to better understand more complex situations, such as charge and energy transport in organic-based devices based on single molecules or bulk materials.

ASSOCIATED CONTENT

Supporting Information

Synthetic procedures, chemical characterizations, EPR characterization of the dications, and details of the quantum-chemical calculations, together with a complete list of authors for some references. This material is available free of charge via the Internet at http://pubs.acs.org.

DOI: 10.1021/ja5125463
J. Am. Chem. Soc. 2015, 137, 3834−3843

AUTHOR INFORMATION

Corresponding Authors

*casado@uma.es
*teodomiro@uma.es
*tsuji@chem.s.u-tokyo.ac.jp
*nakamura@chem.s.u-tokyo.ac.jp

Notes

The authors declare no competing financial interest.

ACKNOWLEDGMENTS

The work at the University of Málaga was supported by MINECO through project reference CTQ2012-33733 and by the Junta de Andalucía through research project P09-FQM-4708, and the work in Tokyo was supported by a Specially Promoted Research Grant (KAKENHI 22000008 to E.N.) and by JST-PRESTO "New Materials Science and Element Strategy" (for H.T.).

REFERENCES

(1) (a) Burroughes, J. H.; Bradley, D. D. C.; Brown, A. R.; Marks, R. N.; Mackay, K.; Friend, R. H.; Burn, P. L.; Holmes, A. B. *Nature* **1990**, *347*, 539−541. (b) Yu, G.; Gao, J.; Hummelen, J. C.; Wudl, F.; Heeger, A. J. *Science* **1995**, *270*, 1789−1791. (c) Hide, F.; Diaz-García, M. A.; Schwartz, B. J.; Andersson, M. R.; Pei, Q.; Heeger, A. J. *Science* **1996**, *273*, 1833−1836. (e) Sariciftci, N. S.; Smilowitz, L.; Heeger, A.; Wudl, F. J. *Science* **1992**, *258*, 1474−1476.

(2) *Handbook of Carbon Nano Materials: Electron Transfer and Applications*; D'Souza, F., Kadish, K. M., Eds.; World Scientific Publishing: Singapore, 2011.

(3) de la Torre, G.; Giacalone, F.; Segura, J. L.; Martín, N.; Guldi, D. M. *Chem.−Eur. J.* **2005**, *11*, 1267−1280.

(4) See, for example: Wieloposki, M.; Molina Ontoria, A.; Schubert, C.; Margraf, J. T.; Krokos, E.; Kirschner, J.; Gouloumis, A.; Clark, T.; Guldi, D. M.; Martin, N. *J. Am. Chem. Soc.* **2013**, *135*, 10372−10381 and references therein..

(5) (a) Zhu, X.; Mitsui, C.; Tsuji, H.; Nakamura, E. *J. Am. Chem. Soc.* **2009**, *131*, 13596−13597. (b) Zhu, X.; Tsuji, H.; López Navarrete, J. T.; Casado, J.; Nakamura, E. *J. Am. Chem. Soc.* **2012**, *134*, 19254−19259.

(6) For heteroatom-containing planar PVs: (a) Yamaguchi, S.; Xu, C.; Tamao, K. *J. Am. Chem. Soc.* **2003**, *125*, 13662−13663. (b) Xu, C.; Wakamiya, A.; Yamaguchi, S. *J. Am. Chem. Soc.* **2005**, *127*, 1638−1639.

(7) (a) Huang, H.; Chen, Z.; Ponce Ortiz, R.; Newman, C.; Usta, H.; Lou, S.; Youn, J.; Noh, Y.-Y.; Baeg, K.-J.; Chen, L. X.; Facchetti, A.; Marks, T. *J. Am. Chem. Soc.* **2012**, *134*, 10966−10973. (b) Ponce Ortiz, R.; Herrera, H.; Seoane, C.; Segura, J. L.; Facchetti, A.; Marks, T. *Chem.—Eur. J.* **2013**, *18*, 532−543.

(8) (a) Sukegawa, J.; Schubert, C.; Zhu, X.; Tsuji, H.; Guldi, D. M.; Nakamura, E. *Nat. Chem.* **2014**, *6*, 899−905. (b) Sukegawa, J.; Tsuji, H.; Nakamura, E. *Chem. Lett.* **2014**, *43*, 699−701.

(9) (a) Horovitz, B. *Solid State Commun.* **1982**, *41*, 729−734. (b) Kuzmany, H. *Phys. Status Solidi B* **1980**, *97*, 521−531. (c) Ehrenfreund, E.; Vardeny, Z.; Brafman, O.; Horovitz, B. *Phys. Rev. B* **1987**, *36*, 1535.

(10) (a) *Vibrational Spectroscopy of New Materials*; Gussoni, M., Castiglioni, C., Zerbi, G., Clark, R. J. H., Hester, R. E., Eds.; Wiley: New York, 1991. (b) Castiglioni, C.; Del Zoppo, M.; Zerbi, G. *J. Raman Spectrosc.* **1993**, *24*, 485−494. (c) Castiglioni, C.; Del Zoppo, M.; Zerbi, G. *Phys. Rev. B* **1996**, *53*, 13319−13325.

(11) For Raman spectroscopic studies of PPV and OPV, see: (a) Zerbi, G.; Galbiati, E.; Gallazzi, M. C.; Castiglioni, C.; del Zoppo, M.; Schenk, R.; Müllen, K. *J. Chem. Phys.* **1996**, *105*, 2509−2516. (b) Tian, B.; Zerbi, G.; Schenk, R.; Müllen, K. *J. Chem. Phys.* **1991**, *95*, 3191−3197. (c) Tian, B.; Zerbi, G.; Müllen, K. *J. Chem. Phys.* **1991**, *95*, 3198−3206. (d) Graham, S. C.; Bradley, D. D. C.; Friend, R. H.; Spangler, C. *Synth. Met.* **1991**, *41*−*43*, 1277−1280.

(12) For Raman spectroscopic studies of doped PPV and OPV, see: (a) Orion, I.; Buisson, J. P.; Lefrant, S. *Phys. Rev. B* **1998**, *57*, 7050−7064. (b) Sakamoto, A.; Furukawa, Y.; Tasumi, M. *J. Phys. Chem. B* **1997**, *101*, 1726−1732. (c) Sakamoto, A.; Furukawa, Y.; Tasumi, M. *J. Phys. Chem. B* **1992**, *96*, 3870−3874.

(13) Lloveras, V.; Vidal-Gancedo, J.; Figueira-Duarte, T. M.; Nierengarten, J.-F.; Novoa, J. J.; Mota, F.; Ventosa, N.; Rovira, C.; Veciana, J. *J. Am. Chem. Soc.* **2011**, *133*, 5818−5833.

(14) Zhu, X.; Tsuji, H.; Nakabayashi, K.; Ohkoshi, S.; Nakamura, E. *J. Am. Chem. Soc.* **2011**, *133*, 16342−16345.

(15) Lee, C. T.; Yang, W. T.; Parr, R. G. *Phys. Rev. B* **1988**, *37*, 785−789.

(16) Frisch, M. J., et al. *Gaussian 09*, revision A.02, Gaussian, Inc.: Wallingford, CT, 2009.

(17) Becke, A. D. *J. Chem. Phys.* **1993**, *98*, 5648−5652.

(18) Francl, M. M.; Pietro, W. J.; Hehre, W. J.; Binkley, J. S.; Gordon, M. S.; Defrees, D. J.; Pople, J. A. *J. Chem. Phys.* **1982**, *77*, 3654−3665.

(19) A complete assignment of the Raman spectrum of **Q(COPV1)** in terms of its theoretical spectrum and vibrational normal modes is provided in Supporting Information (Figure S5 and Table S4).

(20) (a) Choi, S. H.; Kim, B.; Frisbie, D. C. *Science* **2008**, *320*, 1482−1486. (b) Ratner, M. A.; Jortner, J. In *Molecular Electronics*; Ratner, M. A., Jortner, J., Eds.; Blackwell: Oxford, 1997. (c) Davis, W. B.; Wasielewski, M. R.; Ratner, M. A.; Mujica, V.; Nitzan, A. *J. Phys. Chem. A* **1997**, *101*, 6158−6164. (d) James, D. K.; Tour, J. M. *Chem. Mater.* **2004**, *16*, 4423−4435. (e) Klauk, H. *Chem. Soc. Rev.* **2010**, *39*, 2643−2666.

(21) (a) Rodríguez González, S.; Ruiz Delgado, M. C.; Caballero, R.; De la Cruz, P.; Langa, F.; López Navarrete, J. T.; Casado, J. *J. Am. Chem. Soc.* **2012**, *134*, 5675−5681. (b) Hoekstra, R. M.; Telo, J. P.; Wu, Q.; Stephenson, R. M.; Nelsen, S. F.; Zink, J. I. *J. Am. Chem. Soc.* **2010**, *132*, 8825−8827.

(22) (a) Hush, N. S. *Prog. Inorg. Chem.* **1967**, *8*, 391−444. (e) Marcus, R. A.; Sutin, N. *Biochim. Biophys. Acta* **1985**, *811*, 265−322. (b) Robin, M. B.; Day, P. *Adv. Inorg. Chem. Radiochem.* **1967**, *10*, 247−422. (c) Hankache, J.; Wenger, O. S. *Chem. Rev.* **2011**, *111*, 5138−5178. (d) Heckmann, A.; Lambert, C. *Angew. Chem., Int. Ed.* **2012**, *51*, 326−392.

(23) González, S. R.; Ie, Y.; Aso, Y.; López Navarrete, J. T.; Casado, J. *J. Am. Chem. Soc.* **2011**, *133*, 16350−16353.

(24) (a) Kubo, T. *Chem. Lett.* **2015**, *44*, 111−122. (b) Sun, Z.; Ye, Q.; Chi, C.; Wu, J. *Chem. Soc. Rev.* **2012**, *41*, 7857. (c) Abe, M. *Chem. Rev.* **2013**, *113*, 7011. (d) Sun, Z.; Zeng, Z.; Wu, J. *Acc. Chem. Res.* **2014**, *47*, 2582. (e) Lambert, C. *Angew. Chem., Int. Ed.* **2011**, *50*, 1756.

(25) (a) Zheng, X.; Wang, X.; Qiu, Y.; Li, Y.; Zhou, C.; Sui, Y.; Li, Y.; Ma, J.; Wang, X. *J. Am. Chem. Soc.* **2013**, *135*, 14912. (b) Su, Y.; Wang, X.; Zheng, X.; Zhang, Z.; Song, Y.; Sui, Y.; Li, Y.; Wang, X. *Angew. Chem., Int. Ed.* **2014**, *53*, 2857.

(26) (a) Shimizu, A.; Kubo, T.; Uruchi, M.; Yakushi, K.; Nakano, M.; Shiomi, D.; Sato, K.; Takui, T.; Hirao, Y.; Matsumoto, K.; Kurata, H.; Morita, Y.; Nakatsuji, K. *J. Am. Chem. Soc.* **2010**, *132*, 14421. (b) Shimizu, A.; Uruichi, M.; Yakushi, K.; Matsuzaki, H.; Okamoto, H.; Nakano, M.; Hirao, Y.; Matsumoto, K.; Kurata, H.; Kubo, T. *Angew. Chem., Int. Ed.* **2009**, *48*, 5482. (c) Konishi, A.; Hirao, Y.; Nakano, M.; Shimizu, A.; Botek, E.; Champagne, B.; Shiomi, D.; Sato, K.; Takui, T.; Matsumoto, K.; Kurata, H.; Kubo, T. *J. Am. Chem. Soc.* **2010**, *132*, 11021.

(27) (a) Wu, T. C.; Chen, C. H.; Hibi, D.; Shimizu, A.; Tobe, Y.; Wu, Y. T. *Angew. Chem., Int. Ed.* **2010**, *49*, 7059. (b) Shimizu, A.; Tobe, Y. *Angew. Chem., Int. Ed.* **2011**, *50*, 6906. (c) Shimizu, A.; Kishi, R.; Nakano, M.; Shiomi, D.; Sato, K.; Takui, T.; Hisaki, I.; Miyata, M.; Tobe, Y. *Angew. Chem., Int. Ed.* **2013**, *52*, 6076.

(28) (a) Karafiloglou, P. *J. Chem. Educ.* **1989**, *66*, 816−818. (b) Borden, W. T.; Iwamura, H.; Berson, J. A. *Acc. Chem. Res.* **1994**, *27*, 109−116. (c) Borden, W. T. *Diradicals*; Wiley: New York, 1982.

(29) (a) Ortiz, R. P.; Casado, J.; Hernandez, V.; Ortiz, R. P.; Casado, J.; Hernandez, V.; Navarrete, J. T. L.; Viruela, P. M.; Orti, E.; Takimiya, K.; Otsubo, T. *Angew. Chem., Int. Ed.* **2007**, *46*, 9057−9061. (b) Zeng, Z.; Sung, Y. M.; Bao, N.; Tan, D.; Lee, R.; Zafra, J. L.; Lee,

DOI: 10.1021/ja5125463
J. Am. Chem. Soc. 2015, 137, 3834−3843

B. S.; Ishida, M.; Ding, J.; López Navarrete, J. T.; Li, Y.; Zeng, W.; Kim, D.; Huang, K.-W.; Webster, R. D.; Casado, J.; Wu, J. *J. Am. Chem. Soc.* **2012**, *134*, 14513−14525. (c) Zeng, Z.; Lee, S.; Zafra, J. L.; Ishida, M.; Zhu, X.; Sun, Z.; Ni, Y.; Webster, R. D.; Li, R.-W.; López Navarrete, J. T.; Chi, C.; Ding, J.; Casado, J.; Kim, D.; Wu, J. *Angew. Chem., Int. Ed.* **2013**, *52*, 8561−8565. (d) Casado, J.; Patchkovskii, S.; Zgierski, M. Z.; Hermosilla, L.; Sieiro, C.; Moreno Oliva, M.; López Navarrete, J. T. *Angew. Chem., Int. Ed.* **2008**, *47*, 1443−1446.

(30) In Scheme 6a, the relevant molecular orbitals (MOs) involved in double spin polarization are considered: the two singly occupied MOs (degenerate by molecular symmetry) and the highest doubly occupied MO, the HOMO (to a first approach this is enough, but the same can happen with the HOMO − 1, etc.). In the HOMO the two electrons are paired so with spins up and down. If we consider an overall singlet configuration, the two electrons in the two SOMOs must have opposite spins. Spin polarization in the singlet can be seen such that the electron with spin up in the HOMO can be delocalized or occupy the SOMO having the electron with spin down (opposite spin, Pauli's exclusion principle), and this delocalization effect can be equally done for the other electron with spin down in the HOMO over the other SOMO with the spin up. In the triplet, delocalization only applies once. Because electron delocalization decreases electronic repulsion energy, the singlet is stabilized twice over the triplet.

(31) Schleyer, P. v. R.; Maerker, C.; Dransfeld, A.; Jiao, H.; Hommes, N. J. R. v. E. *J. Am. Chem. Soc.* **1996**, *118*, 6317.

DOI: 10.1021/ja5125463
J. Am. Chem. Soc. 2015, 137, 3834−3843